

# Desynchronization Index: a New Approach for Exploring Complex Epileptogenic Networks in Stereoelectroencephalography

Federico Mason<sup>†</sup>, Lorenzo Ferri<sup>†</sup>, Lidia Di Vito, Lara Alvisi, Luca Zanuttini, Matteo Martinoni, Roberto Mai, Francesco Cardinale, Paolo Tinuper, Roberto Michelucci, Elena Pasini\*, Francesca Bisulli\*

**Abstract**—Stereoelectroencephalography (SEEG) is an invasive surgical procedure to record the electrical activities in cortical brain regions, aiming at identifying the Epileptogenic Zone (EZ) in patients with drug-resistant epilepsy. To improve the accuracy of the EZ definition, SEEG analysis can be supported by computational tools, among which the Epileptogenic Index (EI) represents the most common solution. However, the scientific community has still not found an agreement on which quantitative biomarkers can characterize the cortical sites within the EZ. In this work, we design a new algorithm, named Desynchronization Index (DI), to assist neurophysiologists in SEEG interpretation. Our algorithm estimates the effective connectivity between cortical sites and hypothesizes that the EZ is identified by those sites getting abnormally desynchronized from the network during the seizure generation. We test the proposed method over a SEEG dataset of 10 seizures, comparing its accuracy in terms of EZ definition against the EI algorithm and clinical ground truth. Our results indicate that the DI algorithm underscores specific connectivity dynamics that can hardly be identified with a pure visual analysis, increasing sensitivity in detecting epileptogenic cortical sites.

**Index Terms**—Stereoelectroencephalography, epilepsy, seizure, brain connectivity, time-varying networks, phase transfer entropy.

## I. INTRODUCTION

THE localization of the Epileptogenic Zone (EZ) is the fundamental prerequisite for performing epilepsy surgery in people with drug-resistant epilepsy [1]. Ensuring a higher accuracy in the definition of the EZ makes it possible to reduce the extent of the surgery, mitigating the risk of complications or chronic deficits. In the most complex scenario, the EZ

can be identified only through invasive procedures, among which Stereoelectroencephalography (SEEG) represents the most accurate methodology [2].

An SEEG recording involves the surgical implantation of electrodes into the patient's brain, enabling the monitoring of electrical activity from deep cortical regions, which is essential for the identification of the EZ. As a result, SEEG-guided surgical resections lead more than 60% of patients to be seizure-free after the intervention [3]. However, SEEG has the drawback of providing very focused information: if none of the intracranial electrodes intersects the EZ, the procedure may result in an unclear definition of the EZ extension, and consequently, in an unsuccessful epilepsy surgery [4].

Nowadays, clinical interpretation of SEEG is mainly based on visual analysis of the recorded signals, focusing on the early phase of the seizure discharge. The final goal is to define an EZ that can be focal or distributed among multiple cortical structures, a scenario falling under the concept of epileptogenic networks [5]. Accordingly, the above process requires the involvement of highly specialized neurophysiologists and is very expensive in terms of time and human resources. The complexity of SEEG interpretation is exacerbated by the fact that a SEEG implant may include hundreds of recording sites, whose relations and dynamics can hardly be analyzed with a pure visual approach.

In the last years, SEEG interpretation has started being supported by computational tools apt at characterizing the EZ and, more in general, the dynamics leading to seizure generation [6]. In this context, the most common methods are based on the analysis of the SEEG power spectrum, as done in the cases of the Epileptogenic Index (EI) [7] and the Epileptogenic Maps (EMs) [8]. Indeed, the cortical sites being part of the EZ are normally associated with the generation of *fast oscillations*, i.e., electrical activities with frequencies in the gamma range ([30, 100] Hz) and beyond.

Other computational approaches try to model the connectivity relationship between the different cortical sites explored through the same SEEG implant, identifying which brain structures show abnormal behavior. In this field, the first studies have focused on analyzing the electric responses generated through intracranial stimulations, known as Cortico-Cortical Evoked Potentials (CCEPs) [9]. On the other hand, this methodology does not enable capturing the true dynamic of epileptogenic networks because CCEPs are based on non-physiological impulses [10].

Another possibility involves the estimation of the functional connectivity between the cortical sites by analyzing the spec-

This work was partially funded by the European Union, under the Italian National Recovery and Resilience Plan (NRRP) of NextGenerationEU, as part of the RESTART project (PE0000001). <sup>†</sup>These authors are both corresponding. \*These authors contributed equally.

Federico Mason is with Department of Information Engineering, University of Padova, Padova, 35131, Italy (e-mail: federico.mason@unipd.it). Lorenzo Ferri, Lidia Di Vito, Lara Alvisi, Matteo Martinoni, Roberto Michelucci, Elena Pasini, and Francesca Bisulli, are with IRCCS Institute of Neurological Sciences of Bologna, Full Member of the European Reference Network EpiCARE, 40139, Bologna, Italy (e-mail: lorenzo.ferri@ausl.bologna.it, lidia.divito@ausl.bologna.it, lara.alvisi@unibo.it, m.martinoni@isnb.it, roberto.michelucci@isnb.it, elena.pasini@isnb.it, francesca.bisulli@unibo.it). Roberto Mai and Francesco Cardinale are with Claudio Munari Epilepsy and Parkinson Surgery Centre - Niguarda Hospital, 20162, Milan, Italy (e-mail: roberto.mai@ospedaleniguarda.it, francesco.cardinale@ospedaleniguarda.it). Francesco Cardinale is also with Department of Medicine and Surgery, University of Parma, 43126, Parma, Italy. Lara Alvisi, Luca Zanuttini, Paolo Tinuper, and Francesca Bisulli are with Department of Biomedical and Neuromotor Science, Alma Mater Studiorum - University of Bologna, Bologna, 40126, Italy (e-mail: luca.zanuttini@studio.unibo.it, paolo.tinuper@unibo.it).

trum of the electrical signals with which they are associated. In this context, most advanced solutions are based on the analysis of the signal phase, which leads to the advantage of avoiding biases due to differences in the signal amplitude. Two common methodologies for this goal are the Phase Locking Value (PLV) and the Phase Lag Index (PLI), which involve different trade-offs in terms of sensitivity and precision [11].

More recent approaches enable modeling the effective connectivity between the cortical sites, distinguishing the direction of the signal relationships. Under this perspective, the phase analysis can be combined with the Granger Causality (GC) [12], giving rise to Phase Transfer Entropy (PTE), which is a very promising technique for SEEG analysis [13]. Hence, using the metrics derived from the graph theory [14], it is possible to discern the specific roles of the cortical sites that lead to the generation of epileptic discharge.

Although the many connectivity-based approaches for interpreting SEEG signals, the literature often presents discordant findings. Most works agree that the *ictal phase* (i.e., the period involving the seizure discharge) is preceded by a general connectivity reduction, followed by the opposite phenomenon during the discharge propagation [15]. Recently, it has been hypothesized that the EZ presents an abnormal inward information flow during the inter-ictal phase [16], and that the epileptogenic level of each cortical site can be assessed by the connection exerted during the epileptic discharge [17].

In this work, we design a new computational framework for supporting neurophysiologists in SEEG interpretation. Specifically, we develop a new algorithm, named Desynchronization Index (DI), that exploits PTE to estimate the relations between cortical sites and then detect connectivity anomalies in the resulting time-varying network. According to our approach, the EZ is identified by the cortical sites that get abnormally disconnected from the rest of the brain and, thus, assume an independent behavior during the ictal phase. To assess its clinical utility, we test the algorithm over a dataset of 10 seizures and compare its output with a *ground truth* established by two board-certified neurophysiologists.

Overall, the main contributions of this manuscript consist of the following points:

- we design two new connectivity-based metrics, named *synchronization* and *desynchronization levels*, describing the tendency for a cortical site to get control or be disconnected from the rest of the brain;
- we design a new algorithm, named DI, which estimates the epileptogenic degree of cortical sites according to their connectivity dynamics, quantified in terms of desynchronization level;
- we implement the DI algorithm to analyze 10 seizures from 6 consecutive patients with drug-resistant epilepsy who underwent SEEG monitoring;
- we analyze the clinical utility of our method and its main disadvantages and drawbacks in comparison to the EI algorithm and clinical ground truth.

Our results indicate that the combined use of the DI and EI algorithms can offer important support to neurophysiologists for the identification of the EZ. In particular, the DI algorithm underscores anomalous connectivity dynamics which

can hardly be detected by adopting a pure visual analysis or by using EI as a standalone tool. Thus, the proposed technique may be used to identify the cortical regions that, despite not presenting fast oscillations, surround the EZ and play an active role in seizure propagation.

The rest of this manuscript is organized as follows: Sec.II reports the most relevant research works using computational for SEEG interpretation; Sec.III presents the methodology proposed for analyzing SEEG signals and the novel DI algorithm; Sec.IV describes the testing dataset and our evaluation methodology; Sec.V presents the results of the work and discusses their relevance from both a technical and clinical point of view; Sec.VI gives the conclusions and depicts some avenues for future work.

## II. RELATED WORK

In clinical practice, the interpretation of SEEG recordings is mainly based on visual analysis and represents a highly time-consuming process because of the high number of signal components that must be reviewed jointly [18]. Clinically, the most common marker of the seizure onset is given by low-voltage fast activities, which characterize electrical discharges spanning beta frequencies ([13, 30] Hz), usually observed in mesial temporal seizures, and gamma frequencies ([30, 100] Hz), observed in neocortical seizures.

The quantification of fast activities and the dynamics leading to the seizure generation can be achieved by analyzing the SEEG spectrum. Such an approach is followed by the EI algorithm designed by Bartolomei and colleagues in [7]. The latter is the most routinely used method to assist clinicians in the visual SEEG interpretation [19] and, occasionally combined with other biomarkers (as proposed in [20], [21]), has been recognized to provide the best accuracy in terms of both EZ localization and surgical outcome prediction.

While the EI quantifies signal epileptogenicity according to the energy distribution in the frequency domain, other approaches try to estimate the variation in neuronal connectivity during the ictal phase. Many different metrics have been proposed for such a goal, and two popular solutions are the PLV [22] and the PLI [23]. Although both these tools are based on the phase distribution, the PLI offers the advantage of avoiding the noisy information associated with the *volume conduction* [24]. A more advanced method is represented by the PTE [25], which enables the estimation of both the delay and the magnitude of neuronal connections.

Most research works agree that brain connectivity, estimated with the PTE or similar techniques, strongly varies in time and, particularly, reaches its maximum when an individual is asleep [26]. Alongside designing the EI algorithm, Bartolomei and colleagues quantify the SEEG connectivity during the ictal transition by using the nonlinear regression coefficient ( $h_2$ ) [27]. Their results denote that connectivity within the epileptogenic network decreases in the period that foresees the ictal phase [28], [29].

While the  $h_2$  coefficient is agnostic to the signal frequencies, another option is to discern the relationships arising in different frequency bands. For instance, the authors of [30] pre-process SEEG signals in specific sub-bands before estimating

brain connectivity via linear cross-correlation. Tested over a population of patients subjected to intracranial stimulations, the proposed framework shows that seizure frequency is proportional to the outward connectivity of the epileptogenic network. A similar methodology is given in [31], whose authors combine frequency-dependent connectivity with Euclidean distance to estimate the EZ extension.

Other approaches correlate the phase of slow oscillations (< 30 Hz) with the amplitude of fast oscillations (> 30 Hz), as occurred for the Phase Slope Index (PSI) and the Phase Amplitude Coupling (PAC) [32]. Using the PSI to model neural relations, the work of [33] shows that the EZ presents higher outward connectivity when the seizure generates than the resting state. Similar results are observed in [34], whose authors compute the PAC between high (Gamma) and low (Delta and Theta) frequency bands, observing an increase in the EZ connectivity during the ictal phase.

In apparent contradiction with previous works, the authors of [35] assess an increase of the inward connectivity in the EZ during the ictal phase. In this case, SEEG connectivity is estimated via Partial Direct Coherence (PDC) [36], while epileptogenic sites are classified according to an ad hoc clustering algorithm. More recently, a work exploiting Spearman rank correlation [37] to assess the coupling between brain structures has shown good results for both the detection of the EZ and the prediction of surgical outcomes [38].

Although the large variety of works implementing connectivity-based metrics for SEEG interpretation, results from the literature do not lead to an agreement on which biomarkers characterize the cortical sites within the EZ. Initial works show that the ictal transition is characterized by an overall connectivity reduction, but the EZ is often identified by those sites with a higher coupling during the seizure propagation. In this work, we propose a new algorithm that aims at overcoming such questions, by quantifying the epileptogenicity level of SEEG signals in terms of *desynchronization*. With this latter, we denote the tendency of a cortical site to assume an independent electrical behavior that cannot be inhibited by neighboring brain structures.

### III. ANALYTICAL MODEL

In this section, we present the computational tools developed for analyzing SEEG signals. We first describe how SEEG signals are modeled within our framework and introduce the EI algorithm, which represents the state-of-the-art for detecting the EZ. Then, we describe the effective connectivity model that we exploit to infer the relation between different cortical sites starting from their phase distribution. Finally, we present the novel DI algorithm, which evaluates the epileptogenicity level of each cortical site according to its tendency to desynchronize from the overall network.

#### A. Epileptogenic Index

We model a single SEEG recording as a multidimensional signal with  $N$  different components, named *channels*, one for each cortical site analyzed. In the following, we denote by  $\mathcal{N}$  the set of channels and by  $|\cdot|$  the cardinality operator, so that

the number of cortical sites is equal to  $N = |\mathcal{N}|$ . According to our approach, each channel  $x \in \mathcal{N}$  is segmented in multiple overlapping windows  $x(t)$ , with  $t = 0, \Delta t, 2\Delta t, \dots$ , where  $\Delta t$  represents the time-shift between consecutive windows. Given the window duration  $T_{\text{window}}$  and the sampling frequency  $f_s$ , the sample number per window is then given by  $T_{\text{window}}/f_s$ .

The EI algorithm models the SEEG epileptogenicity according to the signal energy in the frequency domain [7]. Given a specific window  $x(t)$ , the algorithm first computes the Fourier Transform (FT) of  $x(t)$ , obtaining a complex value  $X(t, f)$  for each frequency in  $[0, f_s/2]$ . Hence, the *energy ratio* between the high- and low-frequency bands of the target signal  $x$  is computed as

$$E_x(t) = \frac{\int_{B_h} \|X(t, f)\|^2 df}{\int_{B_\ell} \|X(t, f)\|^2 df}, \quad (1)$$

where  $B_h$  and  $B_\ell$  are the high- and low-frequency ranges, while  $\|\cdot\|$  is the norm function.

The straightforward idea behind this technique is that epileptic discharge is characterized by the increase of fast oscillations, which are assessed in terms of signal energy in the high-frequency band. Normalizing the high-frequency by the low-frequency energy, it is possible to compare signals recorded in different cortical sites, which may be characterized by different amplitude and, thus, energy distribution. At the same time, computing the energy ratio for each SEEG channel is not sufficient to determine the EZ: there may be channels that are associated with high energy ratio values even in the absence of epileptic discharges.

To avoid the underlined issue, the EI algorithm considers a CUMulative SUM (CUSUM) control chart to discern the channels with abrupt increases in the energy ratio. Given a sequence of observations  $\omega(t)$ , interspersed by a period  $\Delta t$ , the CUSUM control chart is defined by the function

$$\Gamma_\gamma(\omega(t)) = \begin{cases} \max\left\{0, \Gamma_\gamma(t - \Delta t) + \frac{\omega(t) - \mu_\omega}{\sigma_\omega} - \gamma\right\}, & t > 0; \\ \omega(t), & t = 0; \end{cases} \quad (2)$$

where  $\gamma$  is a tuning parameter that makes the statistic less or more sensitive to the new observations, while  $\mu_\omega$  and  $\sigma_\omega$  are the estimates of the mean and standard deviation of  $\omega$ . In the case of the EI algorithm, the observations  $\omega(t)$  are given by the energy ratio  $E_x$  associated with each channel  $x \in \mathcal{N}$ .

The original version of the EI algorithm does not consider the standard deviation  $\sigma_{E_x}$  in the normalization and dynamically re-estimates the mean  $\mu_{E_x}$  every time the energy ratio varies significantly. Instead, in this work, we propose to estimate both the  $\mu_{E_x}$  and  $\sigma_{E_x}$  statistic by looking at the period immediately preceding the ictal discharge. Practically, for each channel  $x \in \mathcal{N}$ , we compute  $\mu_{E_x}$  and  $\sigma_{E_x}$  over the time interval  $[t_{\text{base}}, t_{\text{start}}]$ , where  $t_{\text{start}}$  is the instant at which the epileptic discharge starts to form. Then, we compute the cumulative sum  $\Gamma_{E_x}(t)$  of the energy ratio  $E_x$  for each time  $t \in [t_{\text{start}}, t_{\text{end}}]$ , where  $t_{\text{end}}$  is the instant at which the epileptic discharge propagates within the overall network.

Given a channel  $x \in \mathcal{N}$  and  $\Gamma_{E_x}(t)$ ,  $\forall t \in [t_{\text{start}}, t_{\text{end}}]$ , we define the *activation time*  $t_{E_x}$  of the channel as the time instant at which  $\Gamma_{E_x}(t)$  reaches the highest value:

$$t_{E_x} = \arg \max_{t \in [t_{\text{start}}, t_{\text{end}}]} \Gamma_{E_x}(t) \quad (3)$$

Besides, we define the *tonicity*  $c_{E_x}$  of the channel as the sum of the energy ratio  $E_x$  computed over the interval following the channel's activation time:

$$c_{E_x} = \int_{t_{E_x}}^{t_{E_x} + \delta} E_x(t) dt, \quad (4)$$

where  $\delta$  is a tuning parameter determining the interval over which  $c_{E_x}$  is computed.

Hence, we can select the  $M$  channels with strongest energy ratio changes by defining the set  $\mathcal{N}_E \subset \mathcal{N}$ , of cardinality  $|\mathcal{N}_E| = M$ , whose elements  $y$  comply with the conditions

$$\Gamma_{E_y}(t_{E_y}) > \Gamma_{E_x}(t_{E_x}), \quad \forall x \in \mathcal{N} \setminus \mathcal{N}_E. \quad (5)$$

Under this perspective,  $M$  denotes the maximum number of epileptogenic channels that are detected by the algorithm. The EI value of each channel  $x \in \mathcal{N}_E$  is then given by

$$EI_x = \frac{c_{E_x}}{t_{E_x} - t_{\text{start}}}, \quad (6)$$

while the EI value of each channel  $x \in \mathcal{N} \setminus \mathcal{N}_E$  is set to 0. We highlight that  $EI_x$  is directly proportional to the channel tonicity  $c_{E_x}$  and decreases as a function of the time difference between the channel activation time  $t_{E_x}$  and the beginning of the ictal phase  $t_{\text{start}}$ .

The above formulation stands out from the original EI algorithm by reducing the number of parameters to be manually set. Particularly,  $t_{\text{start}}$  and  $t_{\text{end}}$  derive from the clinical interpretation of the SEEG recording and denote the period during which the epileptic discharge takes shapes. Instead,  $t_{\text{base}}$  should be defined in such a way to ensure that the statistics  $\mu_{E_x}$  and  $\sigma_{E_x}$  are as accurate as possible. Hence, the only parameters to be tuned are the maximum number  $M$  of epileptogenic channels, the interval  $\delta$  over which the tonicity is computed (used in (4)), and the weight  $\gamma$  of the CUSUM control chart (used in (2)), which trades off between the false alarm and miss-detection probabilities.

## B. Effective Connectivity Model

According to our framework, the characteristics of the epileptogenic sites within a SEEG implant can be assessed by estimating the effective connectivity between the SEEG channels. To pursue such a goal, we consider the PTE algorithm, which, given a couple of channels  $x, y \in \mathcal{N}$  at time  $t$ , models their coupling according to the phase distributions of  $x(t)$  and  $y(t)$ . Under this perspective, PTE may lead to different results depending on the technique used to model the phase distribution.

In this work, we model the phase distributions of the SEEG channels by a modified version of the Freedman-Diaconis rule [39]. Given a specific window  $x(t)$ , we first compute the FT of  $x(t)$ , obtaining  $n = T_{\text{window}}/f_s$  phase values, each associated

with a specific frequency  $f \in [0, f_s/2]$ . Hence, we infer the bin width  $\vartheta$  of the phase distribution  $\theta_x(t)$  as

$$\vartheta = \frac{P_{95}[\theta_x(t)] - P_5[\theta_x(t)]}{\sqrt[3]{n}}, \quad (7)$$

where  $P_{95}[\cdot]$  and  $P_5[\cdot]$  are the functions returning the 95th and 5th percentiles of the input distribution, respectively.

Unlike the original technique proposed by Freedman and Diaconis, we increase the bin width  $h$  to reduce the influence of volume conduction on the connectivity model. The same principle is adopted by the PLI algorithm, which, however, does not consider the effectiveness of the network connection [23]. Besides, PLI presents critical pitfalls, including underestimating the connections associated with small propagation delays or with signals whose phase difference distribution fluctuates around zero. Our technique, instead, tries to act as a compromise between PLI and the PLV, which suffer the effect of volume conduction and, thus, lead to many *type I* errors, i.e., false connectivity phenomena.

Lets denote by  $\theta_x(t)$  and  $\theta_y(t)$  the phase distribution of  $x(t)$  and  $y(t)$ , respectively. According to the PTE algorithm, the connectivity that the channel  $x$  exerts on the channel  $y$  at time  $t$  is proportional to the amount of information in  $\theta_x(t)$  that can be used to predict the future evolution of  $\theta_y(t)$ . Specifically, the phase transfer entropy between  $x(t)$  and  $y(t)$ , considering a lag  $\tau$ , is given by

$$T_{x \rightarrow y}(t, \tau) = I(\theta_y(t), \theta_y(t + \tau)) + I(\theta_x(t), \theta_y(t)) - I(\theta_x(t), \theta_y(t), \theta_y(t + \tau)) - H(\theta_y(t)), \quad (8)$$

where  $H(\cdot)$  and  $I(\cdot)$  denote the entropy and the mutual information functions, respectively.

We observe that the PTE formulation, as reported in (8), is a directed connectivity measure, which means that, in general,  $T_{x \rightarrow y}(t, \tau) \neq T_{y \rightarrow x}(t, \tau)$ . Besides, the value  $T_{x \rightarrow y}(t, \tau)$  depends on the lag  $\tau$ , representing the time distance at which the evolution of  $\theta_y$  is estimated. In order to remove the dependency from  $\tau$ , with a slight abuse of notation, we redefine the phase transfer entropy between  $x(t)$  and  $y(t)$  as the maximum value of  $T_{x \rightarrow y}(t, \tau)$  among multiple lags in the set  $[0, \tau_{\text{max}}]$ :

$$T_{x \rightarrow y}(t) = \max_{\tau \in [0, \tau_{\text{max}}]} T_{x \rightarrow y}(t, \tau). \quad (9)$$

By doing so, we obtain that the magnitude of the effective connection exerted on the channel  $y$  by the channel  $x$  at time  $t$  is given by  $T_{x \rightarrow y}(t)$ , while the propagation delay associated with such a connection is:

$$\tau_{x \rightarrow y}(t) = \arg \max_{\tau \in [0, \tau_{\text{max}}]} T_{x \rightarrow y}(t, \tau). \quad (10)$$

Hence, if  $\tau_{x \rightarrow y}(t) = 0$ , there is a zero-propagation delay for the information flow going from  $x(t)$  to  $y(t)$ .

## C. Desynchronization Index

Given the effective connectivity model designed in Sec.III-B, we aim to design a marker to identify the channels associated with abnormal connectivity behavior. To this goal, we follow the approach presented in [40], where Sparks

and colleagues extended the Exponentially Weighted Moving Average (EWMA) statistic to detect anomalous behaviors in time-varying networks. In particular, our method identifies the generation of the epileptic discharge in terms of abrupt reduction in the communication between the nodes belonging to the EZ and the rest of the network.

Given a sequence of observations  $\omega(t)$ , interspersed by a period  $\Delta t$ , the EWMA control chart is defined by the function:

$$\mathcal{E}_\alpha(\omega(t)) = \begin{cases} \alpha\omega(t) + (1 - \alpha)\mathcal{E}_\alpha(\omega(t - \Delta t)) & t > 0; \\ \omega(t) & t = 0; \end{cases} \quad (11)$$

where  $\alpha \in [0, 1]$  is a tuning parameter that determines the rate at which older information influences the EWMA statistic. In particular, as  $\alpha \rightarrow 1$ , the function gives more importance to the most recent observations, better capturing rapid process changes at the cost of an increased false alarm probability.

In the following, we write  $\mathcal{T}(t)$  to indicate the distribution of the inter-channel connections  $T_{x \rightarrow y}(t)$ ,  $\forall x, y \in \mathcal{N}$ , at time  $t$ . Hence, we denote by  $E[\mathcal{T}(t)]$ ,  $P_{75}[\mathcal{T}(t)]$ , and  $P_{25}[\mathcal{T}(t)]$  the expectation, the 75th percentile, and the 25th percentile of  $\mathcal{T}(t)$ . We use the EWMA algorithm, as defined in Eq.(11), to compute a smoothed version of the above statistics as well as of each connection  $T_{x \rightarrow y}(t)$ ,  $\forall x, y \in \mathcal{N}$ . Then, We define  $\mathcal{N}_x^{\text{in}}(t)$  as the set of channels presenting abnormal inward connectivity with respect  $x$  at time  $t$ :

$$\mathcal{N}_x^{\text{in}}(t) = \{y \in \mathcal{N} : \mathcal{E}_\alpha(T_{y \rightarrow x}(t)) > \mathcal{E}_\alpha(P_{75}[\mathcal{T}(t)]) \text{ or } \mathcal{E}_\alpha(T_{y \rightarrow x}(t)) < \mathcal{E}_\alpha(P_{25}[\mathcal{T}(t)])\}; \quad (12)$$

Similarly, we define  $\mathcal{N}_x^{\text{out}}(t)$  as the set of channels presenting abnormal outward connectivity with respect  $x$  at time  $t$ :

$$\mathcal{N}_x^{\text{out}}(t) = \{y \in \mathcal{N} : \mathcal{E}_\alpha(T_{x \rightarrow y}(t)) > \mathcal{E}_\alpha(P_{75}[\mathcal{T}(t)]) \text{ or } \mathcal{E}_\alpha(T_{x \rightarrow y}(t)) < \mathcal{E}_\alpha(P_{25}[\mathcal{T}(t)])\}. \quad (13)$$

Hence, we define the actual  $\psi_x^{\text{in}}(t)$  and expected  $\hat{\psi}_x^{\text{in}}(t)$  inward connection density of channel  $x$  at time  $t$  as follow:

$$\psi_x^{\text{in}}(t) = \sum_{y \in \mathcal{N}_x^{\text{in}}(t)} \mathcal{E}_\alpha(T_{y \rightarrow x}(t)); \quad (14)$$

$$\hat{\psi}_x^{\text{in}}(t) = |\mathcal{N}_x^{\text{in}}(t)| \cdot \mathcal{E}_\alpha(E[\mathcal{T}(t)]). \quad (15)$$

In an equivalent fashion, we define the actual  $\psi_x^{\text{out}}(t)$  and expected  $\hat{\psi}_x^{\text{out}}(t)$  outward connection density of channel  $x$  at time  $t$  as follow:

$$\psi_x^{\text{out}}(t) = \sum_{y \in \mathcal{N}_x^{\text{out}}(t)} \mathcal{E}_\alpha(T_{x \rightarrow y}(t)); \quad (16)$$

$$\hat{\psi}_x^{\text{out}}(t) = |\mathcal{N}_x^{\text{out}}(t)| \cdot \mathcal{E}_\alpha(E[\mathcal{T}(t)]). \quad (17)$$

We can now define the desynchronization level of a channel  $x \in \mathcal{N}$  at time  $t$  as

$$D_x(t) = \sqrt{\hat{\psi}_x^{\text{in}}(t)} - \sqrt{\psi_x^{\text{in}}(t)}, \quad (18)$$

and the synchronization level of the same channel as

$$S_x(t) = \sqrt{\psi_x^{\text{out}}(t)} - \sqrt{\hat{\psi}_x^{\text{out}}(t)}. \quad (19)$$

Hence, at each time  $t$ ,  $D_x(t)$  represents the tendency for channel  $x \in \mathcal{N}$  to assume an independent behavior, while

$S_x(t)$  represents the tendency for  $x$  to increase its influence over the rest of the network.

We now apply the CUSUM chart to both the desynchronization and synchronization levels, thus obtaining  $\Gamma_{D_x}(t)$  and  $\Gamma_{S_x}(t)$  for each channel  $x \in \mathcal{N}$  and for each time  $t \in [t_{\text{start}}, t_{\text{end}}]$ . Hence, using the equations (3) and (4), we can compute the activation times  $t_{D_x}$  and  $t_{S_x}$  and the tonicities  $c_{D_x}$  and  $c_{S_x}$ ,  $\forall x \in \mathcal{N}$ , considering the desynchronization and synchronization levels instead of the energy ratio.

Following the same approach presented in III-A, we define the set  $\mathcal{N}_D$  and  $\mathcal{N}_S$ , including the  $M$  channels showing the strongest changes in terms of connectivity. Finally, for each channel in  $\mathcal{N}_D$ , we define the DI value as

$$DI_x = \begin{cases} \frac{c_{D_x}}{t_{D_x} - t_{\text{start}}} & x \in \mathcal{N}_D, \\ 0 & x \notin \mathcal{N}_D. \end{cases} \quad (20)$$

Instead, for each channel in  $\mathcal{N}_S$ , we define the Synchronization Index (SI) value as

$$SI_x = \begin{cases} \frac{c_{S_x}}{t_{S_x} - t_{\text{start}}} & x \in \mathcal{N}_S, \\ 0 & x \notin \mathcal{N}_S. \end{cases} \quad (21)$$

Appreciably, the DI and SI algorithms follow the same settings of the EI, making it necessary to tune only three parameters, namely the maximum number  $M$  of epileptogenic channels, the interval  $\delta$ , and the weight  $\gamma$ .

Although this section developed two distinct connectivity-based algorithms for SEEG interpretation, we hypothesize that the epileptogenicity degree of cortical sites can be quantified in terms of desynchronization. Thus, in the rest of the manuscript, we focus on the DI algorithm, while we leave the investigation of the SI algorithm for future work.

#### IV. EVALUATION METHODOLOGY

This section introduces the methodology considered for assessing the utility of the DI algorithm. In the following, we first present the SEEG dataset where our tool is evaluated, describing the SEEG recording process and the patients from both demographic and clinical points of view. Then, we showcase how the EI and DI algorithms are implemented and present the metrics used for determining the performance of these methods in the detection of the EZ.

##### A. Dataset

This study considers a cohort of 8 *consecutive patients* that were monitored through SEEG at IRCCS Institute of Neurological Sciences of Bologna from January 2022 to June 2023. The protocol for the study was approved by the local ethics committee (protocol number 741-2021, committee code 97338), and written informed consent was obtained from each patient participating in the study. In all the cases, the SEEG implant included multiple electrodes, each presenting 5–18 recording sites, named contacts; the number and location of the electrodes were patient-tailored, depending on the EZ localization hypothesis. Particularly, each contact was 22 mm in length and was separated by 1.5 m from neighboring contacts.

TABLE I: Demographic and clinical data\*.

	Patient 0	Patient 1	Patient 2	Patient 3	Patient 4	Patient 5
Sex	Male	Male	Male	Female	Female	Male
Age (SEEG)	39	24	36	52	25	48
Age (Onset)	33	1	16	3	2	22
Handedness	Right	Right	Right	Left	Right	Right
Comorbidity	Migraine	NPRL2 mutation	Lumbosciatica	Postpartum meningitis	Neonatal ischemia	Hip Dysplasia
Semiology	Non-motor unaware	Motor unaware	Motor unaware	Motor unaware	Motor unaware	Motor unaware
EEG topography	Right temporal	Bilateral frontal	Left temporal	Right temporal	Right temporal	Right temporal
MRI findings	Right MTS	Left frontal FCD	Right temporal PB	Right MTS	Right ulegyria	Right MTS
PET hypofixation	Right temporal	Left frontal	Left temporal	Right temporal	Right PTO	Right temporal
Seizure frequency	Weekly	Daily	Monthly	Weekly	Weekly	Weekly
EZ localization	Right temporal	Left orbitofrontal	Left temporal	Right temporal	Right basal temporal	Right temporal
PZ localization	Temporal	Frontal and insular	Temporal	OF and insular	TP and insular	TP and insular
Surgery	Temporal lobectomy	SEEG-guided RF-TC	Temporal lobectomy	Temporal lobectomy	Temporal lobectomy	Temporal lobectomy
Surgical outcome	Seizure free	1 seizure after 1 year	Seizure free	Seizure free	Seizure free	Seizure free
Histology	HS 1	Not available	FCD 1b	HS 1	Aspecific findings	HS 1

\*MTS stays for mesial temporal sclerosis, HS for hippocampal sclerosis FCD for focal cortical dysplasia, RF-TC for radio-frequency thermocoagulation, OF for orbitofrontal, TP for temporoparietal, PTO for parietal-temporal-occipital, PB for Pole Blurring.

The SEEG implantation followed the workflow developed at Niguarda Hospital [41] and involved the construction of a multimodal scene of the patient’s brain. This latter makes it possible, for clinicians, to comprehensively evaluate all the anatomical information regarding the cortical area explored by each contact. Specifically, the SEEG signals were recorded using the Nihon Kohden 2100 polygraph, considering 192 or 256 channels according to the total number of electrical contacts, and a sampling frequency of  $f_s = 1000$  Hz.

Besides the electrical signals, a high-definition synchronized video of each patient was recorded for the whole duration of the SEEG monitoring (up to 20 days per patient), enabling a correlation between electrical and clinical features. Finally, for each patient, it was collected the main demographic and clinical data, such as past medical history, age at disease onset, seizure semiology, neuropsychological examinations, neuroimaging findings (MRI, DTI, PET fMRI), non-invasive electrical recordings, surgical outcomes, follow-up information, and histopathological diagnoses.

From the initial dataset, 2 patients were excluded since, in one case, the EZ was not identified, and, in the other case, a signal artifact precluded the use of our framework to analyze the SEEG data. The final cohort comprises 4 males and 2 females with an average age of 37.3 years (range 24-52) at the time of the recording and 12.8 years (range 1-22) at the time of the disease onset. In five cases, the clinical data pointed to a probable EZ in the temporal lobe (4 right, 1 left), while a single patient had a probable EZ in the frontal lobe (left).

At the time of SEEG implantation, seizure frequency ranged from daily to monthly, depending on the patient. In all cases, the SEEG outcomes enabled the definition of the EZ and, thus, the performing of tailored radio-frequency thermocoagulations, which enabled the control of seizures in a single patient, while the remaining underwent anterior-temporal lobectomy. Histopathological analysis led to clinical results compatible with hippocampal sclerosis in 3 cases, and cortical dysplasia in 1 case. Demographic and clinical details of the studied population are reported in Tab. I.

## B. Performance Evaluation

We assess the performance of the EI and DI algorithms by their ability to correctly identify the channels involved in the

genesis and propagation of the epileptic discharges. Hence, for each patient, we consider all the channels belonging to the EZ as the *ground truth* for the overall analysis. The selection of the EZ channels was performed by two board-certified neurophysiologists (L.D-V. and E.P.), who were blinded to the output of our computational framework.

Up to two seizures per patient are selected, and an SEEG epoch of  $T_{\text{epoch}} = 500$  seconds is analyzed for each seizure, considering the period before the complete diffusion of the epileptic discharge. If multiple seizures were available, we discard the seizures recorded during the first two days of the monitoring period (during which the pharmacological treatment is still active) and those occurring in rapid succession. This was done because the use of anti-epileptic drugs and the outbreak of a seizure cluster may interfere with the normal behavior of the epileptogenic networks.

Before running the EI and DI algorithms, the SEEG signals are pre-processed through a notch filter centered at  $f_{\text{notch}} = 50$  Hz. In the analysis, we exclude the sites exploring the White Matter (WM) since they are not sources of electric signals. The selection of the WM channels was performed by a board-certified neurophysiologist (L.F.), according to the electrical activity of the cortical sites and their localization in the SEEG multimodal scene. No other cortical sites are excluded from the analysis, making our framework agnostic to the specific patient and seizure to be analyzed.

The output of the EI and DI values are normalized in the  $[0, 1]$  interval, and a threshold  $\eta$  (in the same range) is set for classifying a channel as epileptogenic. Hence, the following performance metrics are considered:

- *sensitivity* (or *true positive rate*), which is the ratio between the number of channels correctly classified as epileptogenic by the algorithm and the total number of epileptogenic channels in the SEEG implant;
- *precision* (or *positive predictive value*), which is the ratio between the number of channels correctly classified as epileptogenic by the algorithm and the total number of channels classified as epileptogenic by the algorithm;
- *accuracy*, which is the ratio between the number of channels correctly classified (as epileptogenic or not epileptogenic) by the algorithm and the total number of channels in the SEEG implant.

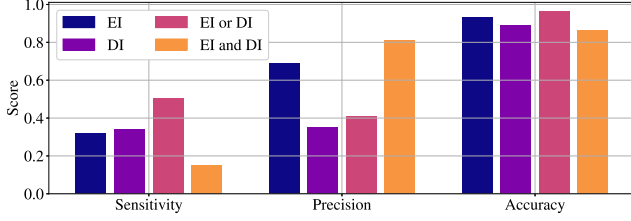


Fig. 1: Performance metrics in the EZ detection.

The EI and DI algorithms are both implemented as standalone tools or combined according to the “and” and “or” Boolean functions. Practically, in the first case (named “EI and DI”), a channel is classified as epileptogenic only if both the algorithms mark it as positive. Instead, in the second case (named “EI or DI”), a channel is classified as epileptogenic if at least one of the algorithms classifies it as positive.

When performing the above analysis, we first consider as ground truth the EZ as defined by the neurophysiologists. Then, the analysis is repeated by considering as a ground truth a subset of the EZ channels, named Detectable Epileptogenic Zone (D-EZ). This latter includes all the EZ channels classified as positive by at least one of the algorithms (i.e., using the EI or DI approach). We observe that this approach makes not possible to describe the algorithms’ performance in absolute terms but only to compare their results.

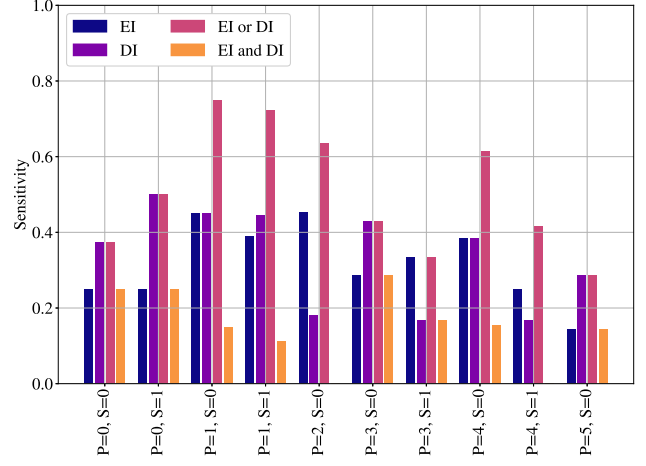
We recall that, while the EZ is the sole responsible for the seizure genesis, other cortical sites may still contribute to its diffusion within the brain, leading to clinical symptoms. Hence, as the last step, we evaluate the two algorithms’ performance in identifying the channels taking part in the propagation of the epileptic discharges. To this goal, we define a new detection class, named Detectable Propagation Zone (D-PZ), that includes all the channels classified as positive by at least one of the algorithms (i.e., using the “EI or DI” approach) and afterward labeled as propagator elements by the two neurophysiologists.

## V. RESULTS

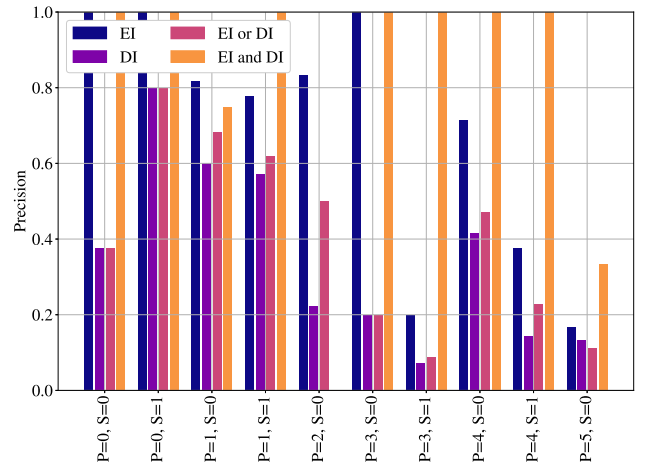
In this section, we present the results obtained when running the EI and DI algorithms in the dataset presented in Sec. IV-A. At first, we specify the settings of our computational framework, and analyze the results according to the metrics given in Sec. IV-B. Hence, we review in more detail two specific seizures among those analyzed, comparing the algorithm outcomes with clinical observations.

### A. Detection Results

The SEEG signals are segmented in time windows lasting  $T_{\text{window}} = 1.00$  s each, considering a time shift of  $\Delta t = 0.25$  s. Given the epoch duration ( $T_{\text{epoch}} = 500$  s) a total of 1996 windows is analyzed for each seizure. For analyzing the windowed signals in the frequency domain and computing the energy ratio, the high- and low-frequency ranges are set to  $B_h = [30.0, 250.0]$  Hz and  $B_\ell = [4.0, 12.0]$  Hz, respectively. Instead, for estimating the connectivity between



(a) Sensitivity.



(b) Precision.

Fig. 2: Performance metrics in the EZ detection, discerning the results for each patient (P) and seizure (S).

different channels according to the PTE algorithm, we consider  $\tau_{max} = 0.20$  s as the maximum propagation delay.

For tuning the algorithms, we set the maximum number of epileptogenic channels to  $M = 15$ , the tonic interval to  $\delta = 5.00$  s (as done in [7]), the weight of the CUSUM chart to  $\gamma = 0.0$ , and the exponential decay of the EWMA chart to  $\alpha = 0.1$ . Moreover, we set the detection threshold of the algorithms to  $\eta = 0.2$ , which implies that we consider as part of the EZ only those channels presenting an epileptogenic value higher than 0.2. Finally, in each epoch, we set the starting time of the baseline period of the CUSUM chart to  $t_{base} = t_{start} - 200.0$  s. This implies that the statistics  $\mu_{E_x}$ ,  $\mu_{D_x}$ ,  $\mu_{S_x}$ ,  $\sigma_{E_x}$ ,  $\sigma_{D_x}$ , and  $\sigma_{S_x}$ ,  $\forall x \in \mathcal{N}$  are estimating according to the signal evolution during the 200.00 s preceding the seizure onset. As explained in Sec. IV,  $t_{start}$  and  $t_{end}$  depend on the specific seizure analyzed and, thus, are epoch-tailored.

In Fig. 1, we report the detection performance of the different algorithms (EI, DI) and their combinations (EI and DI, EI or DI), considering the channels within the EZ as a classification target. We can appreciate that EI and DI lead

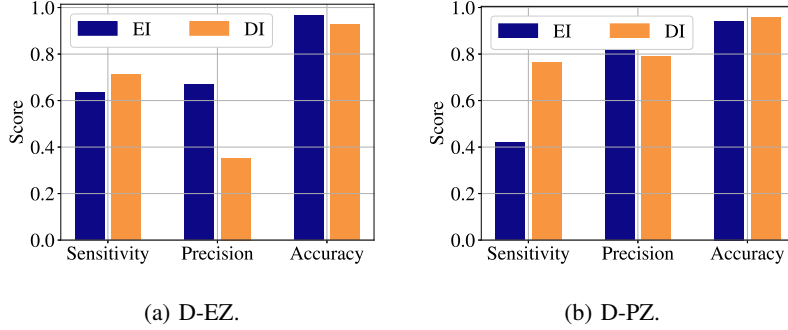
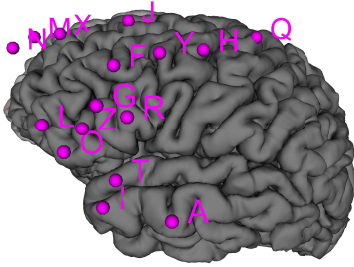
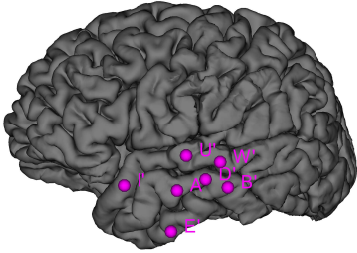


Fig. 3: Performance metrics in the D-EZ and D-PZ detection.



(a) Patient 1.



(b) Patient 2.

Fig. 4: SEEG implants.

to a similar sensitivity (0.32 and 0.34 in the two cases, respectively) when they are used as a standalone tool, while their combination (EI or DI) raises the sensitivity of more than 50% (with a final score of 0.52). This proves that the two algorithms return different sets of results, i.e., the channels associated with a higher EI value are not the same associated with a higher DI value.

Concerning the precision, the EI algorithm leads to the best results (with a score of 0.64), while considering the “and” function for combining the algorithms enables an improvement in the final performance of about 15%. At the same time, the DI algorithm is associated with the worst outcomes, returning a precision of only 0.35, denoting the presence of many false positives. Overall, the detection architecture leading to the best accuracy is given by the “EI or DI” approach (with a score of 0.96), followed by the EI algorithm (with a score of 0.93) and the DI algorithm (with a score of 0.89), respectively.

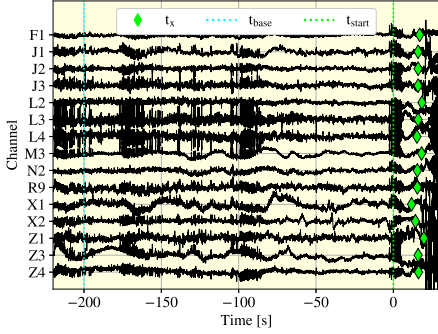
In Fig. 2, we better analyze the results, in terms of sensitivity and precision, associated with each specific patient ( $P$ ) and seizure ( $S$ ). The same dynamics expressed by the aggregated results repeat in almost each specific seizure event. In 7 out of 10 cases, the DI algorithm leads to a higher sensitivity than the EI algorithm and in a single case the combined use of the two systems (through the “EI or DI” approach) does not enable any sensitivity improvement. Focusing on the precision, the EI algorithm always leads to better results than the DI algorithm while, appreciably, the “EI and DI” approach maximizes the precision (up to 1) in all the cases but one.

Finally, in Fig. 3, we report the detection performance considering the channels of the D-EZ and D-PZ zones as a classification target. In this case, the two algorithms are implemented as standalone tools only, without considering the “EI or DI” and “EI and DI” architectures. This is because the D-EZ and D-PZ are defined according to the algorithms’ output, and they include all the epileptogenic and propagation channels that any of the algorithms classify as positive. In both cases, the DI algorithm leads to the best results in terms of sensitivity (0.70 and 0.73, respectively), while the EI algorithm ensures a higher precision. Instead, considering the accuracy as an overall score, the EI algorithm is superior in the D-EZ scenario, while DI outperforms EI in the D-PZ scenario.

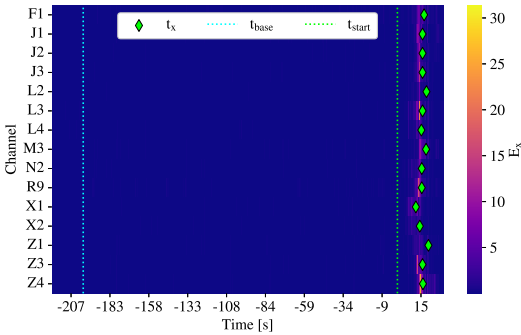
### B. Concordant Example

In the following, we better evaluate the operations of the two algorithms, analyzing two specific seizure events. We first consider patient  $P = 1$ , whose SEEG implant (represented in Fig. 4a) explored the left frontal lobe and the left temporal lobe and includes 171 different recording sites (16 electrodes). In Fig. 5a, we report the bipolar representation of the  $M = 15$  channels associated with the strongest energy ratio variation during the 250 seconds preceding the propagation of the epileptic discharges in the case of seizure  $S = 0$ . Instead, in Fig. 5b, we report the energy ratio values associated with each channel during the same period.

In the two figures, the time is shifted according to the start of the ictal phase, so that  $t_{\text{start}} = 0$  s and  $t_{\text{base}} = -200$  s. In particular,  $t_{\text{base}}$  denotes the time instant from which the baseline statistics of the energy ratio per channel were computed while  $t_{\text{start}}$  denotes the time instant from which the algorithm starts detecting possible signal abnormalities.



(a) Signal.



(b) Energy ratio.

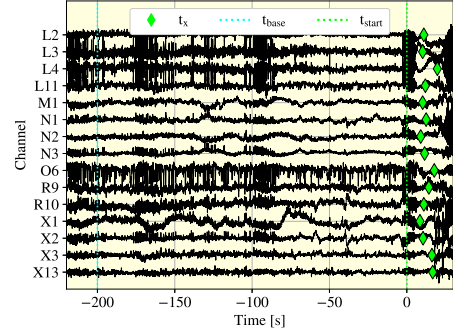
Fig. 5: EI operation in a concordant case.

Finally, the green diamond markers denote the activation times  $t_x, \forall x \in \mathcal{N}$ , at which the energy ratio of each channel maximally diverges from its baseline behavior.

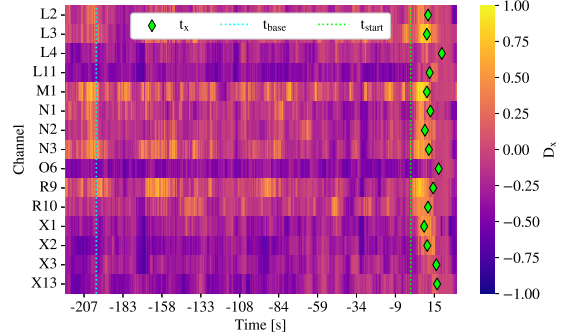
In Fig. 6, we represent the operation of the DI algorithm in the same scenario, using the same settings for the CUSUM chart. Hence, 6a reports the  $M = 15$  channels showing the most significant connectivity changes, while Fig. 6b) reports the desynchronization level for the same channels, highlighting how DI monitors the abnormalities of each channel. Comparing Fig. 6b with Fig. 5b, we can observe that the energy ratio represents a less noisy metric than the desynchronization level. During the baseline interval, the value  $E_x$  associated with each channel  $x \in \mathcal{N}$ , tends to zero. Instead, during the ictal phase ( $t_{\text{start}} > 0$ ), most channels present abrupt energy changes, with a peak  $E_x$  of about 30 for channels L3, R9, and Z4.

The desynchronization level is characterized by a much higher variability during the baseline period since many channels present bursts of reduced connectivity also for  $t_{\text{start}} < 0$ . This suggests that changes in the desynchronization level are not a univocal phenomenon of the epileptic discharge. On the other hand, Fig. 6b highlights how all the channels present a more marked desynchronization phenomenon slightly before the increase of the fast oscillations. Indeed, the average activation time computed according to the DI algorithm is 12.85 s, while the same statistic computed according to the EI algorithm is 15.23 s.

Finally, in Fig. 7, we report the epileptogenicity levels assigned to each channel by the two algorithms as well as the



(a) Signal.



(b) Desynchronization level.

Fig. 6: DI operation in a concordant case.

brain structure with which each channel is associated. In both cases, the algorithms' output is normalized within the  $[0, 1]$  range, so that higher epileptogenic values are associated with a higher influence in the diffusion of the epileptic discharge. We can appreciate that the outputs are mostly concordant as both techniques identify the most epileptogenic channels within the posterior olfactory sulcus, which was deemed responsible for the patient's epilepsy.

### C. Discordant Example

In the following, we consider seizure  $S = 0$  of patient  $P = 2$ , whose SEEG implant (represented in Fig. 4b) explored the right temporal lobe and includes 113 recording sites (7 electrodes). As done previously, we report the  $M = 15$  channels considered as most epileptogenic according to the two approaches, focusing first on the EI algorithm (Fig. 8) and then on the DI algorithm (Fig. 9). As before, the energy ratio associated with each channel presents low values during the baseline period, and then abruptly rises during the ictal phase. Particularly, channels D3 and D4, bordering the hippocampal region, reach a maximum energy ratio of about 40 about 30 seconds after  $t_{\text{start}}$ .

In Fig. 9, we perform the same analysis while considering the desynchronization level as the main epileptogenic marker. We first observe that, in general, the network connectivity is much less noisy than the seizure analyzed in Fig. 6 since the channels do not present prominent connectivity variation during the baseline period. This difference is due to the

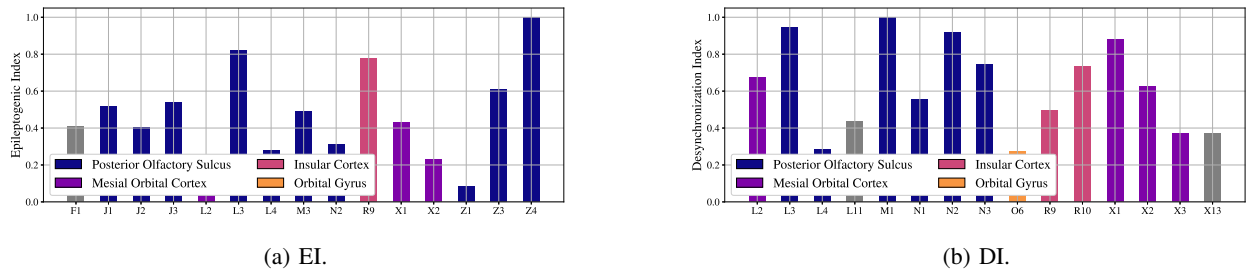
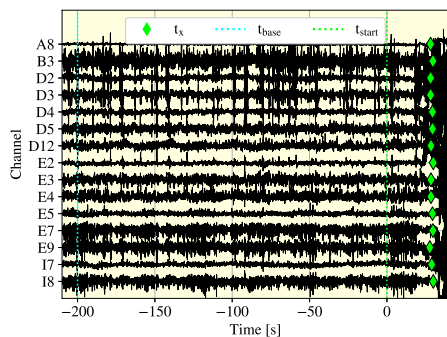
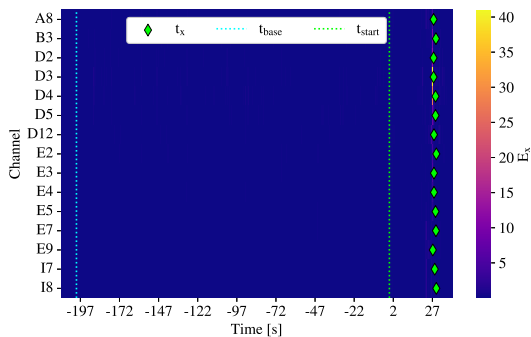


Fig. 7: EI and DI outcomes in a concordant case.

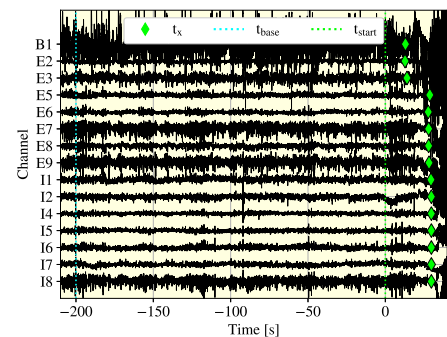


(a) Signal.

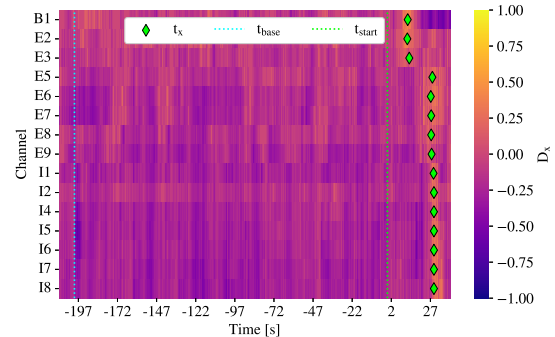


(b) Energy ratio.

Fig. 8: EI operation in a discordant case.



(a) Signal.



(b) Desynchronization level.

Fig. 9: DI operation in a discordant case.

different network sizes: the SEEG implant of patient  $P = 2$  includes almost half of the recording sites of those associated with patient  $P = 1$ . In other words, the network explored is much more focused in this second case and, thus, presents more stable connectivity patterns.

Focus on the ictal phase ( $t_{\text{start}} > 0$ ), we can appreciate that the DI algorithm identifies an early desynchronization phenomenon several seconds before the generation of the fast oscillations. Indeed, as shown in Fig. 9, channels B1, E2, and E3 (which all explore the cortical area neighboring the hippocampus) are characterized by a significant connectivity drop of more than 15 seconds before the increase in the energy ratio. Overall, the average activation time of the channels is 29.10 s in the case of the EI algorithm, and 26.10 s in the case of the DI algorithm. This result confirms that channel

desynchronization is somehow an anticipatory phenomenon, with respect to the increase in the energy ratio, for the genesis of the epileptic discharge.

Finally, Fig. 10 compares the epileptogenicity levels assigned to each channel by the algorithms, also reporting the cortical locations of the channels within the SEEG implants. In this case, the algorithms' output is only partially concordant: both the techniques marked the channels associated with the temporal pole and the collateral sulcus as epileptogenic but seemed to identify the origin of the epileptic discharge in different regions. In particular, the EI algorithm identifies the EZ within the parahippocampal gyrus, as channels D3 and D4 are the only ones associated with an epileptogenic index higher than 0.6. Instead, the DI algorithm underscores channel B1, which is located within the hippocampal head, and channel

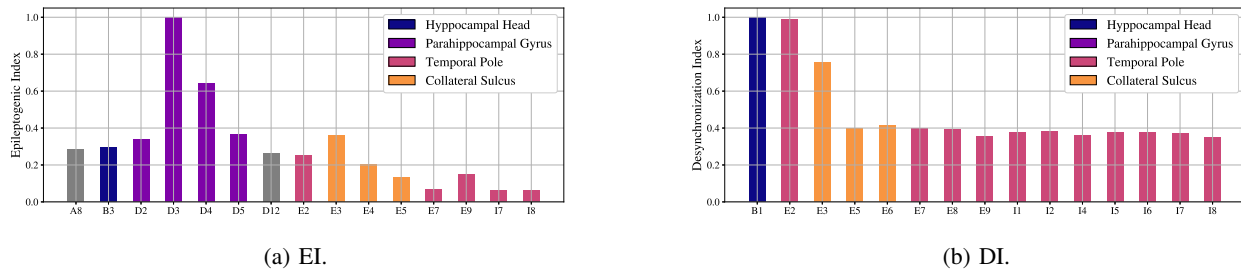


Fig. 10: EI and DI outcomes in a concordant case.

E2, which explores the temporal pole. Such a difference is explained by the fact that the parahippocampal gyrus presents the fastest oscillations (Fig. 8), while the mesial temporal lobe is associated with the desynchronization phenomenon that precedes the epileptic discharges (Fig. 9).

#### D. Clinical Discussion

The above results show that the proposed DI algorithm can recognize the desynchronization phenomena associated with fast oscillations and, thus, the generation of the epileptic discharge. At the same time, our approach also underscores the flattening of SEEG signals that precede the seizure generation in electrodes that intersect or surround the EZ (as observed in Sec. V-C). This leads the DI algorithm to have a partially concordant output with the EI algorithm, which instead focuses on quantifying the magnitude of the high-frequency energy associated with each cortical site.

The DI algorithm, contrary to most state-of-the-art solutions, does not compute the signal energy on specific frequency bands but aims at evaluating the desynchronization level of each SEEG channel. More specifically, DI marks as epileptogenic the cortical sites that abruptly assume a static phase distribution in time and, thus, are not influenced by any other sites explored through the SEEG implant. The key idea behind the proposed method is that the epileptogenic signals present an independent behavior that is anomalous within the network and cannot be inhibited by the other cortical structures.

According to our approach, desynchronization phenomena constitute a characterizing factor of both the sites associated with fast oscillations and the areas neighboring the EZ. This is in line with the most recent findings in the field of EZ detection and confirms that the generation of epileptic seizures is allowed by a connectivity reduction in the overall network. In particular, during the inter-ictal phase, the regions surrounding the EZ may assume an inhibitory function that prevents the diffusion of the epileptic discharges and, thus, constitute a key component of the epileptogenic network.

In a clinical context, the DI algorithm can help neurophysiologists identify the cortical regions that surround the EZ and contribute to the propagation of epileptic discharges. In particular, DI emphasizes phenomena that are not marked by other computational techniques, such as the EI algorithm, and are not easy to identify by a pure visual analysis. Hence, the combined use of the DI and the EI algorithms can strongly increase the sensitivity in the EZ detection, although

marking as epileptogenic also cortical sites that are not part of the EZ. From this perspective, the clinical judgment of neurophysiologists remains an essential element for discerning false positive outcomes.

We finally observe that the proposed DI algorithm may also reflect the presence of ictal activities in cortical areas not directly explored by the SEEG implant. This may be useful in scenarios where the SEEG signal does not enable the clear visualization of the seizure generation and propagation. Hence, our technique may help neurophysiologists to discern whether the epileptogenic network is totally or only partially explored by the SEEG implant and, thus, the information obtained by the SEEG monitoring is sufficient to ensure, with high probability, the success of epilepsy surgery.

## VI. CONCLUSION

In this work, we developed a new computational framework for analyzing SEEG signals, with the final goal of identifying the EZ in patients with drug-resistant epilepsy. Our method, named DI, exploits the PTE model to estimate the effective connectivity between the cortical sites explored by the same SEEG implant and estimates the tendency of each site to behave independently from the rest of the network. Particularly, the DI algorithm identifies as most epileptogenic the SEEG channels that present an abrupt desynchronization in the period immediately preceding the ictal phase.

To evaluate its clinical utility, we implemented the DI algorithm over a dataset of 10 seizures from 6 patients with drug-resistant epilepsy who underwent SEEG monitoring. Hence, we computed the algorithm accuracy in identifying the cortical sites that are part of the EZ or contribute to the seizure propagation, considering the EI algorithm as a benchmark approach. Our results denoted that DI shows higher sensitivity than EI, and the best accuracy is obtained when combining the two algorithms as a unique detection tool.

The proposed approach, integrated with other quantitative biomarkers, may constitute a key support for SEEG interpretation. Indeed, DI underscores signal modifications not visually evident, helping to identify those sites that contribute to the seizure propagation or inhibit the epileptic discharge during the inter-ictal period. In future work, we intend to clinically validate the DI algorithm over a wider dataset, possibly including data from different clinical research centers, and evaluate the potential of our computational framework for analyzing SEEG signals during the inter-ictal period.

## REFERENCES

- [1] H. O. Lüders, I. Najm, D. Nair, P. Widdess-Walsh, and W. Bingman, "The epileptogenic zone: general principles," *Epileptic Disorders*, vol. 8, no. 2, pp. 1–9, Aug. 2006.
- [2] J. Isnard *et al.*, "French guidelines on stereoelectroencephalography (SEEG)," *Neurophysiologie Clinique*, vol. 48, no. 1, pp. 5–13, Feb. 2018.
- [3] M. Cossu, F. Cardinale, L. Castana, A. Citterio, S. Francione, L. Tassi, A. L. Benabid, and G. L. Russo, "Stereoelectroencephalography in the presurgical evaluation of focal epilepsy: a retrospective analysis of 215 procedures," *Neurosurgery*, vol. 57, no. 4, pp. 706–718, Oct. 2005.
- [4] F. Cardinale, M. Cossu, L. Castana, G. Casaceli, M. P. Schiariti, A. Miserocchi, D. Fuschillo, A. Moscato, C. Caborni, G. Arnulfo *et al.*, "Stereoelectroencephalography: surgical methodology, safety, and stereotactic application accuracy in 500 procedures," *Neurosurgery*, vol. 72, no. 3, pp. 353–366, Mar. 2013.
- [5] F. Bartolomei *et al.*, "Defining epileptogenic networks: contribution of SEEG and signal analysis," *Epilepsia*, vol. 58, no. 7, pp. 1131–1147, Jul. 2017.
- [6] V. Gnatkovsky *et al.*, "Biomarkers of epileptogenic zone defined by quantified stereo-EEG analysis," *Epilepsia*, vol. 55, no. 2, pp. 296–305, Feb. 2014.
- [7] F. Bartolomei, P. Chauvel, and F. Wendling, "Epileptogenicity of brain structures in human temporal lobe epilepsy: a quantified study from intracerebral EEG," *Brain*, vol. 131, no. 7, pp. 1818–1830, Jul. 2008.
- [8] O. David *et al.*, "Imaging the seizure onset zone with stereoelectroencephalography," *Brain*, vol. 134, no. 10, pp. 2898–2911, Oct. 2011.
- [9] C. J. Keller *et al.*, "Mapping human brain networks with cortico-cortical evoked potentials," *Philosophical Transactions of the Royal Society B: Biological Sciences*, vol. 369, no. 1653, pp. 1–14, Oct. 2014.
- [10] S. Dionisio *et al.*, "Connectivity of the human insula: a cortico-cortical evoked potential (CCEP) study," *Cortex*, vol. 120, pp. 419–442, Nov. 2019.
- [11] K. Gupta, P. Grover, and T. J. Abel, "Current conceptual understanding of the epileptogenic network from stereoelectroencephalography-based connectivity inferences," *Frontiers in Neurology*, vol. 11, no. 569699, pp. 1–7, Nov. 2020.
- [12] A. Shojaie and E. B. Fox, "Granger causality: A review and recent advances," *Annual Review of Statistics and Its Application*, vol. 9, no. 1, pp. 289–319, Mar. 2022.
- [13] M.-y. Wang *et al.*, "Identification of the epileptogenic zone of temporal lobe epilepsy from stereo-electroencephalography signals: A phase transfer entropy and graph theory approach," *NeuroImage: Clinical*, vol. 16, pp. 184–195, Jul. 2017.
- [14] F. Panzica, G. Varotto, F. Rotondi, R. Spreafico, and S. Franceschetti, "Identification of the epileptogenic zone from stereo-EEG signals: a connectivity-graph theory approach," *Frontiers in Neurology*, vol. 4, no. 175, pp. 1–6, Nov. 2013.
- [15] T. Proix, F. Bartolomei, M. Guye, and V. K. Jirsa, "Individual brain structure and modeling predict seizure propagation," *Brain*, vol. 140, no. 3, pp. 641–654, Mar. 2017.
- [16] K. M. Gunnarsdottir *et al.*, "Source-sink connectivity: A novel interictal EEG marker for seizure localization," *Brain*, vol. 145, no. 11, pp. 3901–3915, Nov. 2022.
- [17] G. Nithin, P. Sathidevi, and P. Ameer, "Graph energy based centrality measures to detect epileptogenic focal invasive EEG electrodes," *Seizure*, vol. 85, pp. 127–137, Feb. 2021.
- [18] F. Bartolomei, A. Nica, M. P. Valenti-Hirsch, C. Adam, and M. Denuelle, "Interpretation of SEEG recordings," *Neurophysiologie Clinique*, vol. 48, no. 1, pp. 53–57, Dec. 2017.
- [19] J. Makhalova *et al.*, "The role of quantitative markers in surgical prognostication after stereoelectroencephalography," *Annals of Clinical and Translational Neurology*, vol. 10, no. 11, pp. 2114–2126, Nov. 2023.
- [20] H. Parasuram, S. Gopinath, A. Pillai, S. Diwakar, and A. Kumar, "Quantification of epileptogenic network from stereo EEG recordings using epileptogenicity ranking method," *Frontiers in Neurology*, vol. 3, no. 12, pp. 1–13, Nov. 2021.
- [21] A. Balatskaya *et al.*, "The 'Connectivity Epileptogenicity Index'(cEI), a method for mapping the different seizure onset patterns in StereoElectroencephalography recorded seizures," *Clinical Neurophysiology*, vol. 131, no. 8, pp. 1947–1955, Aug. 2020.
- [22] J.-P. Lachaux, E. Rodriguez, J. Martinerie, and F. J. Varela, "Measuring phase synchrony in brain signals," *Human Brain Mapping*, vol. 8, no. 4, pp. 194–208, Nov. 1999.
- [23] C. J. Stam, G. Nolte, and A. Daffertshofer, "Phase lag index: assessment of functional connectivity from multi channel EEG and MEG with diminished bias from common sources," *Human Brain Mapping*, vol. 28, no. 11, pp. 1178–1193, Nov. 2007.
- [24] L. R. Peraza, A. U. Asghar, G. Green, and D. M. Halliday, "Volume conduction effects in brain network inference from electroencephalographic recordings using phase lag index," *Journal of Neuroscience Methods*, vol. 207, no. 2, pp. 189–199, Jun. 2012.
- [25] M. Lobier, F. Siebenhühner, S. Palva, and J. M. Palva, "Phase transfer entropy: a novel phase-based measure for directed connectivity in networks coupled by oscillatory interactions," *Neuroimage*, vol. 85, no. 2, pp. 853–872, Jan. 2014.
- [26] P. Bourdillon, B. Hermann, M. Guénot, H. Bastuji, J. Isnard, J.-R. King, J. Sitt, and L. Naccache, "Brain-scale cortico-cortical functional connectivity in the delta-theta band is a robust signature of conscious states: an intracranial and scalp EEG study," *Scientific Reports*, vol. 10, no. 14037, pp. 1–13, Aug. 2020.
- [27] F. Wendling, J.-J. Bellanger, F. Bartolomei, and P. Chauvel, "Relevance of nonlinear lumped-parameter models in the analysis of depth-EEG epileptic signals," *Biological Cybernetics*, vol. 83, no. 4, pp. 367–378, Oct. 2000.
- [28] F. Bartolomei, F. Wendling, J.-J. Bellanger, J. Régis, and P. Chauvel, "Neural networks involving the medial temporal structures in temporal lobe epilepsy," *Clinical Neurophysiology*, vol. 112, no. 9, pp. 1746–1760, Sep. 2001.
- [29] F. Wendling, F. Bartolomei, J.-J. Bellanger, and P. Chauvel, "Interpretation of interdependencies in epileptic signals using a macroscopic physiological model of the EEG," *Clinical Neurophysiology*, vol. 112, no. 7, pp. 1201–1218, Jul. 2001.
- [30] M. Daoud *et al.*, "Stereo-EEG based personalized multichannel transcranial direct current stimulation in drug-resistant epilepsy," *Clinical Neurophysiology*, vol. 137, pp. 142–151, May 2022.
- [31] J. M. Bernabei *et al.*, "Electrocorticography and stereo EEG provide distinct measures of brain connectivity: implications for network models," *Brain Communications*, vol. 3, no. 3, pp. 1–11, Jul. 2021.
- [32] A. M. Bastos and J.-M. Schoffelen, "A tutorial review of functional connectivity analysis methods and their interpretational pitfalls," *Frontiers in Systems Neuroscience*, vol. 9, no. 175, Jan. 2016.
- [33] H. Jiang *et al.*, "Interictal SEEG resting-state connectivity localizes the seizure onset zone and predicts seizure outcome," *Advanced Science*, vol. 9, no. 2200887, pp. 1–11, Jun. 2022.
- [34] X. Liu, F. Han, R. Fu, Q. Wang, and G. Luan, "Epileptogenic zone location of temporal lobe epilepsy by cross-frequency coupling analysis," *Frontiers in Neurology*, vol. 12, no. 764821, pp. 1–14, Nov. 2021.
- [35] N. An, X. Ye, Q. Liu, J. Xu, and P. Zhang, "Localization of the epileptogenic zone based on ictal stereo-electroencephalogram: Brain network and single-channel signal feature analysis," *Epilepsy Research*, vol. 167, pp. 1–10, Nov. 2020.
- [36] L. A. Baccalá and K. Sameshima, "Partial directed coherence: a new concept in neural structure determination," *Biological Cybernetics*, vol. 84, no. 6, pp. 463–474, Jun. 2001.
- [37] J. H. Zar, "Spearman rank correlation," *Encyclopedia of Biostatistics*, vol. 7, Jul. 2005.
- [38] Y. Huang *et al.*, "Intracranial electrophysiological and structural basis of BOLD functional connectivity in human brain white matter," *Nature Communications*, vol. 14, no. 3414, pp. 1–9, Jun. 2023.
- [39] D. Freedman and P. Diaconis, "On the histogram as a density estimator: L<sub>2</sub> theory," *Zeitschrift für Wahrscheinlichkeitstheorie und verwandte Gebiete*, vol. 57, no. 4, pp. 453–476, Dec. 1981.
- [40] R. Sparks and J. D. Wilson, "Monitoring communication outbreaks among an unknown team of actors in dynamic networks," *Journal of Quality Technology*, vol. 51, no. 4, pp. 353–374, Oct. 2019.
- [41] F. Cardinale *et al.*, "Cerebral angiography for multimodal surgical planning in epilepsy surgery: description of a new three-dimensional technique and literature review," *World Neurosurgery*, vol. 84, no. 2, pp. 358–367, Aug. 2015.